

# Towards Real-time Registration of 4D Ultrasound Images

Pezhman Foroughi, Purang Abolmaesumi\* and Keyvan Hashtrudi-Zaad

**Abstract**—In this paper, we demonstrate a method for fast registration of sequences of 3D liver images, which could be used for the future real-time applications. In our method, every image is elastically registered to a so called fixed ultrasound image exploiting the information from previous registration. A few feature points are automatically selected, and tracked inside the images, while the deformation of other points are extrapolated with respect to the tracked points employing a fast free-form approach. The main intended application of the proposed method is real-time tracking of tumors for radiosurgery. The algorithm is evaluated on both naturally and artificially deformed images. Experimental results show that for around 85 percent accuracy, the process of tracking is completed very close to real time.

## I. INTRODUCTION

Fast registration of sequences of ultrasound images acquired in real-time can play an important role for radiation therapy. Currently, computed tomography (CT) and fluoroscopy are the common imaging techniques employed for radiation therapy of abdominal tumors. The tumors are often not clearly distinguishable in CT and fluoroscopes and usually, metal clips are implanted around the tumor that are visible in these imaging modalities [1], [2]. Implanting metal markers is an invasive procedure, and fluoroscopy exposes the patient to extra radiation. Ultrasound imaging has no ionizing radiation, therefore, an alternative solution exploiting 3D real-time ultrasound imaging is of high interest.

Ultrasound images can be employed to compensate for the deformations of soft tissue. The treatment could be planned on preoperative MR/CT image, and implemented by registering a selected intra-operative ultrasound image called “fixed image” to the preoperative MR/CT image. After registration, the location of tumor could be determined inside the fixed ultrasound image. The tumor might not be clearly visible inside the ultrasound images, but the position of the tumor could be estimated through time by registering the current image referred to as “moving image” to the fixed image. Besides radiosurgery, sequential registration of liver images could be used for tissue elasticity analysis, as well as liver biopsy [3], [4].

Great amount of work has been dedicated to temporal registration of cardiac images mainly as a tool for motion analysis. A sequence of 3D MR images of heart is considered as one 4D image in [5], and images are registered all at once. The method is aimed for off-line cardiac motion analysis. A

free-form registration technique is also developed using B-splines models for Cardiac MR sequences [6]. Semi-local spatio-temporal parametric model for the deformation using splines along with global optimization is employed in [7] to register a sequence of 2D cardiac ultrasound images. Speckle tracking is also used for temporal registration of cardiac images [8]. In [9], vessels extracted from X-ray angiography sequences are matched spatio-temporally. Tracking liver motions in MR/CT images during respiration has also been investigated [10].

Recently, 4D ultrasound imaging has become available, and it is foreseeable that in the near future, real-time access to 3D ultrasound data with high update rates will be possible for many users. This will introduce a wide range of new applications for ultrasound imaging.

In this paper, we propose a method of 4D registration of ultrasound images of liver. The developed methodology stems from our previous registration algorithm introduced in [11], and has been adapted to register a sequence of ultrasound images to a fixed image. The main idea is to utilize the information from registration from prior volumes to decrease the registration time and dependency of registration to maximum displacement. The method is evaluated using both simulated and real ultrasound images of volunteers’ livers during several breathing cycles. Our analyses suggest that without any significant change in the amount of error, the registration process is significantly sped up.

## II. METHOD

Fig. 1 shows the various stages of the registration procedure utilizing the information from the last registration and the fixed image.

### A. Preprocessing and Calculation of Attribute Vectors

There are a number of steps that need to be taken for the registration. Each time a new image from the sequence of images arrives, it first goes through a preprocessing stage of noise reduction and contrast adjustment. A low-pass filter is needed since the first and the second derivatives of the images are calculated later in the process. In the current implementation, we simply pass the image through a Gaussian filter as the low-pass filter.

Afterwards, for each voxel in the image, a feature vector called “attribute vector” is calculated, which is a variation of attribute vector introduced in [12]. The vector contains the intensity of the voxel, the magnitude of the gradient, and the second derivative (Laplacian of the Gaussian). It highlights important features of the ultrasound images such as boundaries of organs and vessels.

P. Foroughi and K. Hashtrudi-Zaad are with the Electrical and Computer Engineering Department, Queen’s University, Canada

\*P. Abolmaesumi (corresponding author) is with the School of Computing and the Electrical and Computer Engineering Department, Queen’s University, Canada; Email: purang@cs.queensu.ca

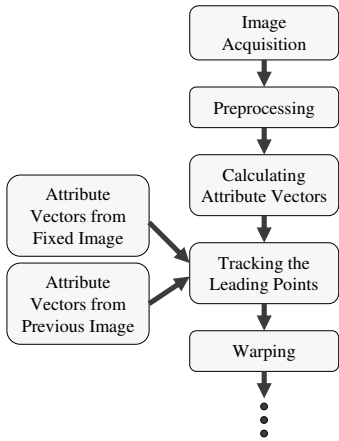


Fig. 1. The acquired images are processed in stages of registration. The attribute vectors calculated from the previous and the fixed image are used for tracking the leading points.

The registration steps are slightly different for the fixed image which is the first image in the sequence. The filtering and calculation of attribute vector set is the same, but the attribute vectors are stored in memory, and are used for the rest of the registration process. In addition, some key points on this image referred to as “leading points” are automatically selected and stored. To select these points, weighted sum of the elements of the attribute vector for each point (referred to as importance function) is computed. The points that their importance function is higher than a threshold are selected as leading points. Such points are usually placed on the distinguishable features of the image.

The selected leading points are tracked through the images, and the other voxels in the images are warped based on the registration of these points. This process shows the importance of leading points. The index of the points that are not robustly tracked are automatically removed from the index list created for this purpose. The details of leading point elimination is provided in Section II-C.

### B. Energy Function

After preprocessing every image, there are three sets of attribute vectors stored in the memory. The first belongs to the fixed image and the other two are for the current and the previous moving images. Moreover, the program saves two sets of points in the memory: the leading points and their corresponding points calculated for the last image. At the beginning, the two sets of points and the three sets of attribute vectors are identical. To find the correspondence in the current image, an energy function is defined for these values:

$$\begin{aligned}
 En_k(P^t) &= \frac{\sum_i w(i)[1 - Sim(P^t(i), LP_k^0(i))]}{2 \sum_i w(i)} \\
 &+ \frac{\sum_i w(i)[1 - Sim(P^t(i), LP_k^{t-1}(i))]}{2 \sum_i w(i)}, (1)
 \end{aligned}$$

where  $En_k(P^t)$  is the energy function of point  $P^t$  on the  $t$ th image for the  $k$ th leading point;  $P^t(i)$  belongs to the

current image and is located at a cubic matching region with  $P^t$  at the center;  $LP_k^{t-1}(i)$  is a point on the previous image at the same location on the matching region with the  $k$ th corresponding leading point on the previous image at the center;  $LP_k^0(i)$  is a point on the fixed image at the same location with respect to the  $k$ th leading point; and  $w_i$  is a convex weight function which is maximum at the center of the matching region.

$Sim(a, b)$  denotes the similarity of points  $a$  and  $b$  from two images, and is defined the same as the similarity function in [11]:

$$Sim(a, b) = \prod_{i=1}^n (1 - \|e_i(a) - e_i(b)\|)^{\alpha_i}, \quad (2)$$

where  $e_i(x)$  is the  $i$ th element of the attribute vector assigned to voxel  $x$ , and  $\alpha_i$  is the contribution of the  $i$ th element of the attribute vector in the similarity function. The similarity function is between zero (no similarity) and one (absolutely similar) since the difference between maximum and minimum of the elements of similarity function is one.

To find the point on the current image which corresponds to the  $k$ th leading point, energy function of all the points inside a spherical search area is calculated. The center of this area is the location of the  $k$ th corresponding point found on the previous image. The voxel with minimum energy function is selected as the new corresponding point.

Assuming that the maximum displacement between the two consecutive images is limited, since the center of search area is picked from the previous image, a small search radius could be selected. Choosing a small search radius increases the speed of the algorithm drastically. Two other factors, in addition to search radius, have large effect on the running time of the algorithm, which will be discussed in Section III-C.

Two similarities are measured in (1): the similarity of the examination point on the current image with leading point on the fixed image, and the similarity of the examination point with the tracked leading point on the previous image. The first one eliminates the possible drifts when the leading points are tracked in the images and ensures that the accuracy of the technique remains unchanged as more images are being registered to the fixed image. The second increases the robustness of the algorithm as the correspondence between the two consecutive images is determined with more accuracy, especially for the images that are largely deformed from the fixed image.

### C. Point Elimination

Some of the leading points may move out of the volume scanned by the ultrasound transducer and therefore, cannot be tracked anymore. Hence, the leading points that are very close to the image boundaries are automatically excluded. An index list is created for the leading points and each time that one point is eliminated, the index list is updated. On the other hand, some of the features in the images may disappear due to shadowing effect. To compensate for this effect, the leading points with energy function higher than a threshold

are also eliminated. The threshold could be easily set since there is a drastic change in the energy function value when a feature disappears. Due to the eliminations, after a while, only the leading points that can be robustly registered are kept.

#### D. Warping

The displacement of the voxels are determined with respect to the displacement of the leading points. Each voxel is displaced inversely proportional to a function of its distance to the leading points faded with a Gaussian function. Warping is the bottleneck for this technique, even though a relatively fast method of warping is selected. However, it is not necessary to warp all the images, and depending on the application, some of images can be selected to be warped.

### III. RESULTS

The current implementation is in MATLAB<sup>TM</sup>, and the computationally heavy functions are written in C++ using “MATLAB<sup>TM</sup> mex functions”. For all the experiments, a 2.8 GHz Pentium 4 with 4 GB of RAM is used.

#### A. Image Acquisition

The sequences of images were captured using the 4D mode of a GE Voluson 730 Expert ultrasound machine with a RAB4-8P transducer. For each set of data, a 4D image with image rate of 4 Hz, depth of 16.9 cm, and sweeping angel of 35 degrees was acquired. Each 4D image consisted of 57 to 64 3D volumes. The volume size for all the experiments was 199x155x93 voxels with a scale factor of 0.74 mm/voxel for all dimensions. The images were taken from the liver of three healthy males  $M_1$  to  $M_3$ . Each series of images contains several number of breathing cycles. The operator tried to keep the ultrasound transducer still during the scanning and to keep the pressure constant, so that the main source of deformation would be breathing. The transducer is oriented so that the displacement of most of the features remain inside the capturing volume. Image acquisition must be much faster than the breathing cycle to avoid volume distortion. Ideally, the volume should be captured all at once, which is not feasible at the moment with the required size of the volumes. Hence, the imaging parameters are selected to create a balance between the size of the volumes and the acquisition time.

#### B. Results for Naturally Deformed Images

The experiments were carried out for the sequences of images taken from all the subjects. Fig. 2 shows three slices of original volumes from subject  $M_1$  taken at different intervals of breathing cycles along with the same slices of the volumes registered to the fixed image. The figure also shows that after a few breathing cycles, the registration performance remains unchanged. For this sequence of images, the volunteer was asked to breath slightly deeper than in a normal respiration in order for deformations to be large and thus the effect of registration becomes more noticeable. The white arrows are positioned at the same location for all the images to make the comparison easier.

#### C. Simulation Results

To simulate the deformation, the matrix of displacement vectors generated from the previous experiment at the maximum deformation was used to create a sequence of deformed images. The displacement was linearly interpolated from zero to the maximum deformation, and was applied to the fixed image to generate a sequence of 10 gradually deforming volumes. Then, the images were registered back using the proposed method, and the overall resulting displacement matrix for the 10th volume was compared to the original matrix.

It is crucial to select the right registration parameters that satisfy the required speed and accuracy based on the application needs. Table I shows how the error and registration time are affected when changing the matching radii in energy function. The tracking time is defined as the total time required to register all the leading points between two consecutive volumes. From this table, it can be concluded that without a significant change in error, the tracking time could notably be decreased by reducing the matching radius.

TABLE I  
EFFECT OF MATCHING RADIUS ON TRACKING TIME

Matching Radius (voxel)	Mean Error (mm)	Tracking Time (sec)
1	3.23	0.97
2	3.01	4.52
3	2.95	12.39
4	2.89	25.42
5	2.93	49.12
6	2.98	68.05

The other factor that has a significant impact on the tracking time is the number of leading points (LPs) selected on the fixed image. By decreasing the number of LPs, the tracking time reduces proportionally. However, it should be ensured that enough LPs are selected on the key features inside the images. To reduce the number of LPs, once a leading point is selected, no more LPs are chosen within a spherical area around that leading point. By increasing the radius of this sphere (LP radius), the number of LPs is decreased as well as the tracking time. Table II shows that the error remains within an acceptable range for reasonably low number of LPs.

TABLE II  
EFFECT OF NUMBER OF LPs ON TRACKING TIME

LP Radius (voxel)	Mean Error (mm)	Tracking Time (sec)	Number of LPs
2	2.67	21.74	205
4	2.89	25.30	237
6	2.97	12.53	118
8	3.02	6.58	61
12	3.08	1.42	13
15	3.86	0.54	5

Since the displacement matrix from subject  $M_1$  produces the highest error and the maximum deformation, it has been used as the worst case for generating Tables I and II. The

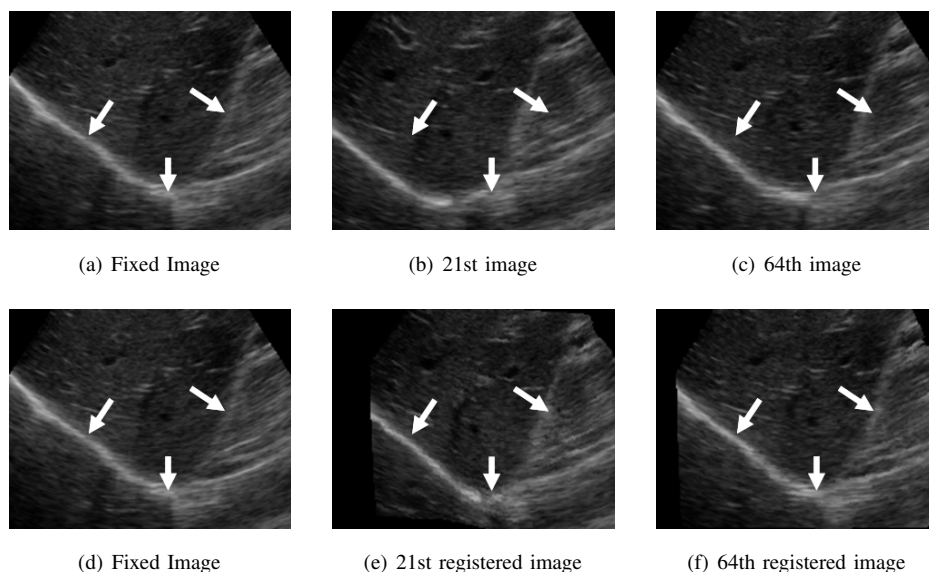


Fig. 2. a) to c) are the slices of the original volumes taken at different periods of breathing cycle, whereas d) to f) are the same slices in the registered volumes. The white arrows are at the same location in all the images.

LP Radius and Matching Radius has been chosen to be 4 voxels for these two tables.

The simulation results for three displacement matrices from subjects  $M_1$  to  $M_3$  are presented in Table III. Based on results from Tables I and II, to preserve the robustness of the technique and to reduce the tracking time, LP Radius and Matching Radius are selected to be 8 and 2, respectively.

TABLE III

RESULTS OF SIMULATIONS WITH THREE DISPLACEMENT MATRICES

	Average Displacement (mm)	Mean Error (mm)	Tracking Time (sec)
$M_1$	16.97	2.89	1.07
$M_2$	10.88	1.51	0.68
$M_3$	12.54	1.72	0.93

For each pair of consecutive volumes, in the current implementation, preprocessing and calculation of attribute vectors, which is written in MATLAB™m-file format, takes about 8.8 seconds, and warping takes about 20 seconds for 60 leading points. However, these times could be reduced significantly using software optimization and hardware acceleration. For instance, GPU could be employed to increase the speed of warping.

#### IV. CONCLUSION

We proposed a novel method for temporal registration of sequences of 3D ultrasound images. The technique was evaluated using both artificially and naturally deformed images. Our analyses led us to a set of registration parameters that provide short tracking time while maintaining high registration accuracy. Tracking is currently performed reasonably fast, whereas the preprocessing and warping could be accelerated exploiting code optimization, multiprocessing and hardware acceleration. Future work includes real-time implementation of the entire registration process and

extensive validation experiments to make the technique more suitable for clinical applications.

#### REFERENCES

- [1] J. Brewer, M. Betke, D. P. Gierga, and G. T. Y. Chen, "Real-time 4D tumor tracking and modeling from internal and external fiducials in fluoroscopy," in *Med. Image Comp. & Comp. Assist. Interventions (MICCAI)*, 2004, pp. 594–601.
- [2] H. Shirato *et al.*, "Four-dimensional treatment planning and fluoroscopic real-time tumor tracking radiotherapy for moving tumor," *Int. J. Radiation Oncology Biol. Phys.*, vol. 48, no. 2, pp. 435–442, 2000.
- [3] A. P. King, J. M. Blackall, G. P. Penney, and D. J. Hawkes, "Tracking liver motion using 3-D ultrasound and a surface based statistical shape model," in *Math. Methods Biomed. Image Anal.*, Desember 2001, pp. 145–152.
- [4] J. M. Blackall, G. P. Penney, A. P. King, and D. J. Hawkes, "Alignment of sparse freehand 3-D ultrasound with preoperative images of the liver using models of respiratory motion and deformation," *IEEE Trans. Image Process.*, vol. 24, no. 11, pp. 1405–1416, November 2005.
- [5] D. Shen *et al.*, "Consistent estimation of cardiac motions by 4D image registration," in *Med. Image Comp. & Comp. Assist. Interventions (MICCAI)*, 2005, pp. 902–910.
- [6] D. Perperidis, R. Mohiaddin, and D. Rueckert, "Spatio-temporal free-form registration of cardiac MR image sequences," in *Med. Imag. Comp. & Comp. Assist. Interventions (MICCAI)*, 2004, pp. 911–919.
- [7] M. J. Ledesma-Carbayo *et al.*, "Spatio-temporal nonrigid registration for ultrasound cardiac motion estimation," *IEEE Trans. Med. Imag.*, vol. 24, no. 9, pp. 1113–1126, 2005.
- [8] X. Chen *et al.*, "Temporal and spatial registration for cardiac strain rate imaging," in *IEEE Symp. on Ultrasonics*, vol. 2, 2003, pp. 2134–2137.
- [9] J. Gu, C. Toumoulin, and H. Shu, "Spatio-temporal registration in coronary angiography," in *IEEE Eng. Med. Biol. (IEMBS)*, vol. 1, 2003, pp. 584–587.
- [10] T. Rohlfing, C. Maurer, J. O'Dell, and J. Zhong, "Modeling liver motion and deformation during the respiratory cycle using intensity-based free-form registration of gated MR images," in *Proc. Int. Soc. Opt. Eng. (SPIE)*, 2001, pp. 337–348.
- [11] P. Foroughi and P. Abolmaesumi, "Elastic registration of 3d ultrasound images," in *Med. Image Comp. & Comp. Assist. Interventions (MICCAI)*, 2005, pp. 83–90.
- [12] D. Shen and C. Davatzikos, "HAMMER: hierarchical attribute matching mechanism for elastic registration," *IEEE Trans. Med. Imag.*, vol. 21, no. 11, pp. 1421–1439, 2002.